A negative ion TPC with GridPix readout

C. Ligtenberg[a,*], M. van Beuzekom[a], Y. Bilevych[b], K. Desch[b], H. van der Graaf[a], F. Hartjes[a], K. Heijhoff[a,b], J. Kaminski[b], P.M. Kluit[a], N. van der Kolk[a], G. Raven[a], J. Timmermans[a]

[a] *Nikhef, Science Park 105, 1098 XG Amsterdam, The Netherlands*
[b] *Physikalisches Institut, University of Bonn, Nussallee 12, 53115 Bonn, Germany*

Abstract

The performance of GridPix technology as a negative ion TPC readout was studied using a quad module with four Timepix3 based GridPix chips. The TPC is operated using a 93.6/5.0/1.4 gas mixture of $Ar/iC_4H_{10}/CS_2$ with a small amount of oxygen and water vapour at a pressure of 1030 mbar and a temperature of 297 K. Tracks were produced by a pulsed N_2 laser. The GridPix chips are sensitive to single drift ions, and allow for the determination of the drift distance using the minority carrier(s). The 1.56 ns time resolution of the Timepix3 chips allows for a precise determination of the drift properties in the longitudinal direction. The measured mobility of majority ion charge carriers is $(1.391 \pm 0.003)\,cm^2/V/s$. Using the high granularity pixel readout, the transverse and longitudinal diffusion coefficients were measured to correspond to an effective thermal diffusion temperature of 305 K and 383 K respectively.

Keywords: Micromegas, gaseous pixel detector, micro-pattern gaseous detector, Timepix, GridPix, negative ion time projection chamber

1. Introduction

In a negative ion Time Projection Chamber (TPC), ionisation charge is transported to the readout plane by negatively charged ions instead of electrons, thereby reducing the diffusion down to the thermal limit [1]. The TPC detects interactions that create ionisation electrons in the gas of the TPC. The primary ionisation electrons are captured by the highly electronegative CS_2 gas component, and the ions formed drift to the anode by a drift field. In the high field amplification region near the anode, the electrons detach and an avalanche occurs which is detected by the readout electronics.

A negative ion TPC was applied to directional dark matter searches, e.g. in the Drift IId experiment [2]. The TPC was operated using a low pressure 30:10 Torr CF_4:CS_2 gas mixture. If oxygen is present in the gas mixture, extra species of ions called minority carriers with a larger mobility are created [3]. From the difference in arrival time, the absolute position in the drift direction

*Corresponding author. Telephone: +31 20 592 2000
Email address: cligtenb@nikhef.nl (C. Ligtenberg)

can be reconstructed without the need of knowing the event time in the detector [4].

In this paper an exploratory study of GridPix technology as a negative ion TPC readout is presented. A GridPix consists of a CMOS pixel chip with integrated amplification grid added by MEMS postprocessing techniques [5, 6]. Recently a quad module with four Timepix3 based GridPix chips was developed in the context of a future collider experiment [7]. The GridPix TPC readout has a fine granularity of 55 µm × 55 µm and is sensitive to single charge carriers. A negative ion TPC with GridPix readout can provide an excellent spatial resolution without a magnetic field. The high single ion resolution of the quad detector allows an accurate measurement of the resolution and an experimental test of the expected low diffusion coefficient for ions. This first investigation focuses on operation of the quad module in an already existing setup at atmospheric pressure.

2. Quad detector

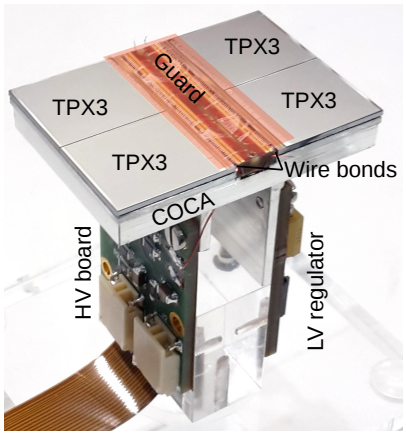

Figure 1: Picture of the quad module with four Timepix3 GridPixes (TPX3) mounted on a cold carrier plate (COCA). The central guard was omitted to show the wire bond PCB, and its operating position is indicated with a transparent rectangle. On the right the Low Voltage (LV) regulator is partially hidden behind the stump, and on the left the High Voltage (HV) board and the flexible Kapton cable are visible. This picture was previously published in [7].

2.1. Gridpix

The GridPix is based on the Timepix3 chip [8], which has 256 × 256 pixels with a pitch of 55 µm × 55 µm. On the surface of the chip a 4 µm thick silicon-rich silicon nitride protection layer is deposited in order to prevent damage to the readout electronics from discharges of the grid. On top of that, 50 µm high

SU8 pillars support a 1 µm thick aluminium grid with 35 µm diameter circular holes aligned to the pixels. The Timepix3 chip has a low equivalent noise charge ($\approx$ 70 e-) and can measure a precise Time of Arrival (ToA) using a 640 MHz TDC. The Timepix3 chip has a data driven readout, and is connected to a speedy pixel detector readout (SPIDR) board at a speed of 160 Mbps [9].

2.2. Quad module

The quad shown in Figure 1, consists of four GridPix chips and is optimised for a high fraction of sensitive area of 68.9%. The external dimensions are 39.6 mm $\times$ 28.38 mm and it can be tiled to cover arbitrarily large areas. The four chips which are mounted on a cooled base plate (COCA), are connected with wire bonds to a common central 6 mm wide PCB. A 10 mm wide guard electrode is placed over the wire bonds 1.1 mm above the grids, in order to prevent distortion of the electric drift field. On the other side, the PCB is connected to a low voltage regulator. The grids are connected by 80 µm insulated copper wires to a high voltage (HV) filtering board. The module consumes about 8 W of power of which 2 W in the LV regulator.

2.3. Experimental setup

The quad module is embedded in a box with 7 other quad modules, resulting in a total of 32 chips. When the measurements were taken, one single quad module with 4 chips could be read out per SPIDR board. Hardware to simultaneously read out multiple quad modules with one SPIDR board is under development. A schematic drawing of the setup is shown in Figure 2. The internal dimensions of the box are 79 mm $\times$ 192 mm $\times$ 53 mm, and it has a maximum drift length (distance between cathode and readout anode) of 40 mm. The drift field is shaped by a series of parallel CuBe field wires of 50 µm diameter with a wire pitch of 2 mm and guard strips are located on all of the four sides of the

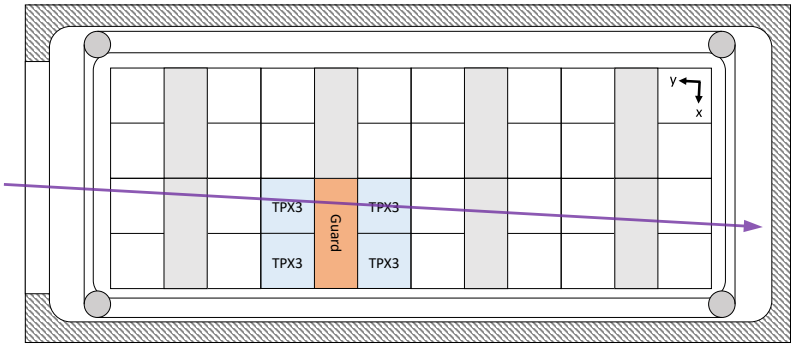

Figure 2: Schematic drawing of the 8-quad module detector with one quad in operation. In purple the laser track direction is indicated.

active area. In addition, six guard wires are suspended over the direct boundaries of the chips at a distance of 1.10 mm–1.18 mm from the grid planes . The box has one Kapton window and three optical glass windows (type H-K9L) to facilitate laser measurements.

The gas volume of 780 ml is continuously flushed with a 93.6/5.0/1.4 gas mixture of $Ar/iC_4H_{10}/CS_2$ at atmospheric pressure. The gas is argon based because of the dual use of the setup for detector development for future colliders, the isobutane gas was added as a quencher to absorb UV photons produced in the avalanches, and the CS_2 concentration is chosen high enough to capture electrons shortly after the ionisation ($\lesssim 200\,\mu m$). A small amount of oxygen (650 ppm–1150 ppm) and water vapour (about 4000 ppm) are present in the drift volume because of diffusion and outgassing of some of the materials. A few ppb of tetra-methyl-phenyleen-diamine (TMPD) molecules are added to enhance laser ionisation in the gas. During data taking, the temperature was 297 K and the pressure was 1030 mbar. The experimental parameters are summarised in Table 1.

The grid voltage is set to $-380\,V$ providing an amplification field strength of $76\,kV/cm$. A hit is registered if the charge on a pixel pad is above the threshold set to 55 DAC counts or about $515\,e^-$. The mean time over threshold of the selected hits is $0.45\,\mu s$. From this, the gain can be determined to be approximately 1000 and the detection efficiency is expected to be 60%. A higher gain and detection efficiency might be achieved by making the grid voltage more negative.

Tracks of ionisation are created by a pulsed 337 nm N_2 laser at a rate of 2.5 Hz with a pulse duration of 1 ns [10]. The laser is operated using the MOPA (Master Oscillator Power Amplifier) principle to obtain a beam near the diffraction limit. The parallel beam can accurately be directed in the gas volume by means of two remotely controlled stages.

Data was taken in a series of nine automated experimental runs. During a run, the drift field was set to a specific strength and the beam was positioned at six different drift distances 6 mm apart and at four different x-positions. Measurements of 2400 laser shots per run are taken in a time frame of approximately 17 minutes.

Table 1: Overview of the experimental parameters. The ranges indicate the variation over the total data taking time

Number of runs	9
Run duration	17 minutes
E_{drift}	100 – 500 V/cm
V_{grid}	$-380\,V$
Threshold	$515\,e^-$
Temperature	295.9 – 297.0 K
Pressure	1030 – 1029 mbar
Oxygen concentration	650 – 1150 ppm
Water vapour concentration	~ 4000 ppm

3. Analysis

In the analysis the laser position is compared to the reconstructed position from the quad detector. The laser track is defined by the recorded stage position as a line parallel to the y-axis. The per pulse variations are smaller than 15 µm. The recorded stage position is taken as the reference to which the four chips are aligned by rotation in two dimensions, and shifts in the two dimensions perpendicular to the laser beam. The position of detected ionisation in the pixel plane is a direct translation from the pixels column (x-direction) and row number (y-direction). To reduce noise, only hits with a time over threshold above 0.1 µs are considered. From the known laser pulse time, the z-position can be calculated as the product of the measured drift time t and the drift velocity v_{drift}. To clean up further the data set, hits are required to be within 2 mm of a laser track in the x-direction and to be within 5 mm of the laser track in the z-direction. The alignment and the measurement of the drift velocity is an iterative process.

An example of a resulting drift time spectrum is shown in Figure 3 for the run at a drift field strength E_{drift} of 300 V/cm. Other experiments using low pressure gas mixtures containing CS_2 and oxygen could distinguish three different minority carriers as separate peaks in the drift time spectrum [3]. In contrast, in our measurements only one secondary peak can be found, which is slightly broader than the first one. This could be due to e.g. overlapping drift time distributions, the much lower oxygen concentration, or the much higher water vapour concentration in our gas mixture affecting the minority carrier(s) production.

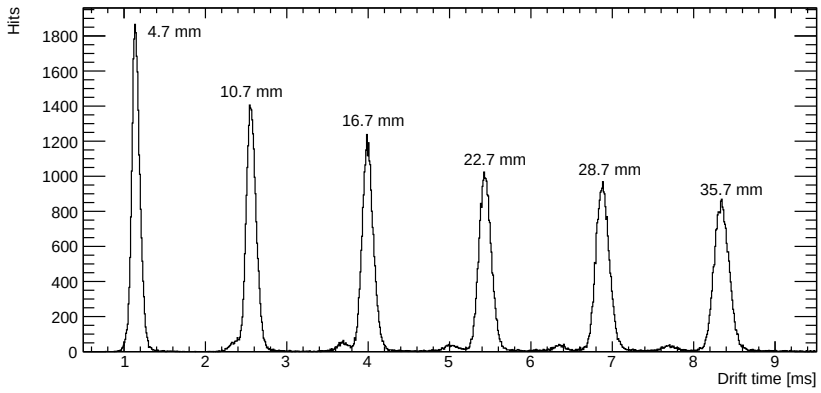

Figure 3: Drift time distribution for 400 laser pulses per z-position, annotated with the drift distance as recorded by the laser stage.

In order to determine the drift properties, a 'global' fit is made per run with measurements at different drift distances for a given electric field strength. The drift time t is fitted with a combination of two Gaussian distributions per laser

z-position:

$$g(t) = n_{\text{hits}} \left[\frac{f_1}{\sigma_1 \sqrt{2\pi}} \exp\left(-\frac{(t-\mu_1)^2}{2\sigma_1^2} \right) + \frac{f_2}{\sigma_2 \sqrt{2\pi}} \exp\left(-\frac{(t - r_2\mu_1)^2}{2\sigma_2^2} \right) + \frac{f_{\text{noise}}}{u_{\text{width}}} \right], \tag{1}$$

where n_{hits} is the number of hits, u_{width} is the width of a uniform distribution set to the fit t range and f_1 is the fraction of the number of detected ions from majority carrier(s) given by $f_1 = 1 - f_2 - f_{\text{noise}}$. Four parameters are different for each drift distance, and two parameters are the same for all drift distances. The mean time μ_1, the standard deviation of the majority carrier distribution σ_1, the standard deviation of the minority carrier(s) distribution σ_2 and the fraction of the number of ions in the flat noise distribution f_{noise}, are fitted per drift distance. In the fit, the fraction of the number of ions from minority carrier(s) f_2 and the ratio of majority carrier mobility to the minority carrier(s) mobility r_2 are equal for all drift distances.

4. Performance

4.1. Number of hits

The mean total number of detected hits per laser pulse is 43. The number of hits can be tuned by adjusting the laser intensity, and the spread on the number of hits is dominated by per pulse variations of the laser intensity. In this gas, a minimum ionising particle is expected to create about 100 ionisation pairs per cm of which about 60 will be detected as hits per cm, because of the 60 % efficiency at a gain of 1000. An example event display for ionisation for a single laser pulse is shown in Figure 4.

4.2. Drift velocity measurements

The average drift times for the majority and minority charge carrier(s) are plotted as a function of the drift distance in Figure 5 for a drift field strength of 300 V/cm. The drift velocity of the minority carrier is found to be 8.1% higher than that of the majority carrier.

The drift velocity of the majority carrier v_{drift} as function of the electric field is shown in Figure 6. The mean measured mobility is $(1.391 \pm 0.003)\,\text{cm}^2/\text{V/s}$. The uncertainty of the measured mobility is estimated as the r.m.s. of the given values, and is probably dominated by fluctuations in the (local) temperature and gas composition. Because of the unique gas composition the mobility cannot directly be compared to the results from other experiments. However, the mobility is the same order of magnitude as previous measurements using gas mixtures containing CS_2 and argon [1], and mixtures containing CS_2 and helium [11].

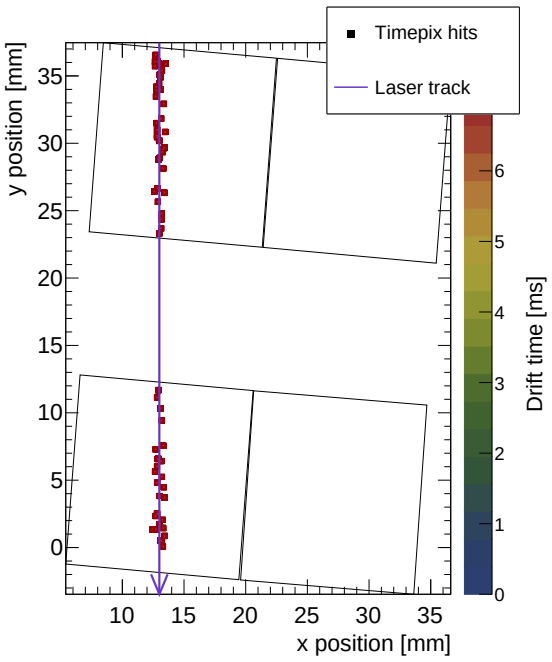

Figure 4: Example of the detected ionisation from one laser pulse with 64 hits in total. The position of the laser track (purple line) and chip edges (black outlines) are drawn in global coordinates. The pixel hits are not to scale.

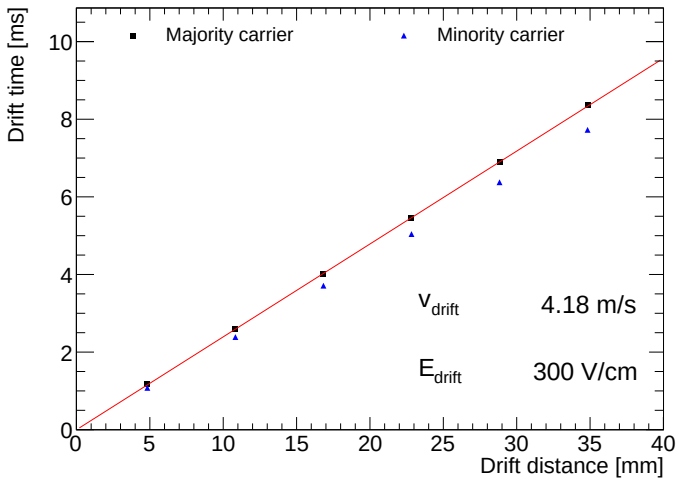

Figure 5: Drift time as a function of z-position for the majority and minority carriers

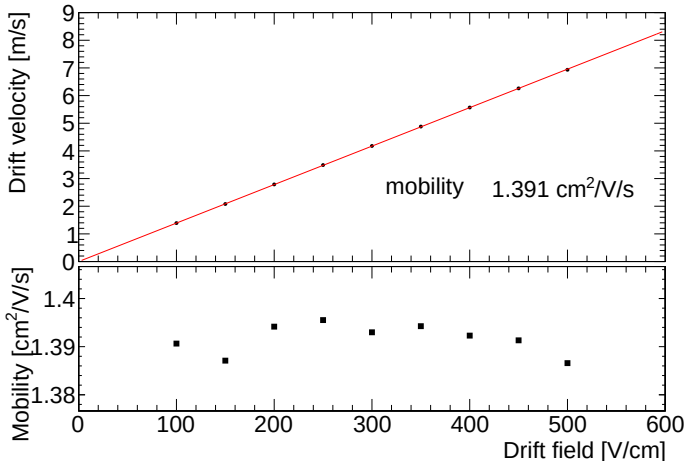

Figure 6: Drift velocity of the majority carrier ion as a function of the drift field. The mobility is acquired from a straight line fit constrained to pass through the origin (0,0).

4.3. Diffusion measurements

As the ions drift towards the readout plane, they diffuse which gives them a Gaussian spread in the longitudinal and transverse direction. The amount of diffusion is characterised by the standard deviation of the Gaussian distribution σ_i, where i stands for the longitudinal direction z or the transverse direction x. This can be expressed as

$$\sigma_i^2 = \sigma_{i0}^2 + D_i^2 z, \tag{2}$$

where σ_{i0} is the standard deviation at zero drift, D_i the diffusion coefficient, and z the drift distance.

The standard deviation is acquired from a fit to the data of one Gaussian in the transverse direction, or the sum of two Gaussian functions in the longitudinal direction, see Equation (1). The drift time is converted to a distance using the measured drift velocity v_{drift}. As an example, the standard deviation as a function of drift distance for the run at a drift field strength E_{drift} of 300 V/cm is shown in Figure 7.

The constant contribution in Equation 2 is roughly independent of the electric field, and on average found to be $\sigma_{x0} = (94 \pm 3)\,\mu\text{m}$ in the transverse direction which can predominantly be attributed to the laser beam width plus some small per shot variation. In the longitudinal direction $\sigma_{z0} = (141 \pm 8)\,\mu\text{m}$ is measured on average over all runs. This can predominantly be attributed to the laser beam width plus per shot variations, the spread on the distance traveled by electrons before they are captured by the CS_2 molecules or unrecognised minority carrier(s).

The diffusion coefficient depends on the electric field strength, and the measurements are shown in Figure 8. At low drift field strengths, the ions have

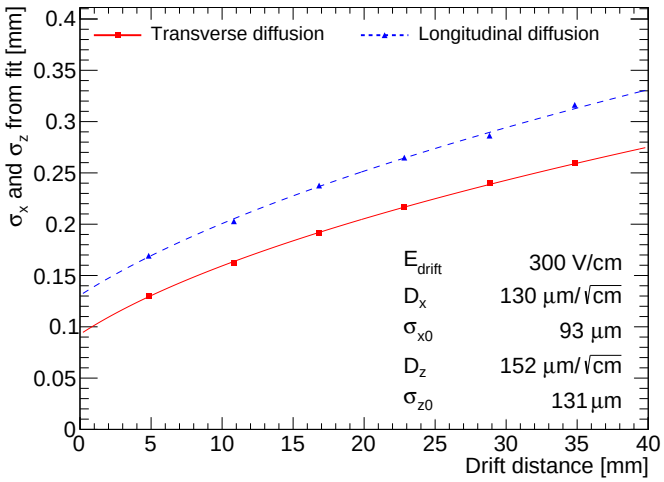

Figure 7: Standard deviation of hit positions in the transverse and longitudinal direction as a function of drift distance for the run with $E_{\mathrm{drift}} = 300\,\mathrm{V/cm}$. The data is fitted with Equation (2).

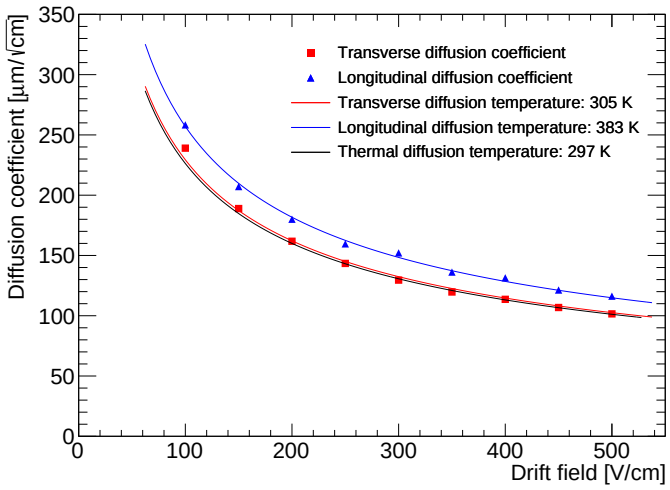

Figure 8: Diffusion coefficients in the longitudinal and transverse directions as a function of the drift field E. Both are fitted with Equation (3). For comparison the expectation for thermal diffusion is shown.

thermal energy and the diffusion coefficient can be expressed as

$$D_{\text{thermal}} = \sqrt{\frac{2k_{\text{B}}T}{eE}}, \tag{3}$$

where k_{B} is the Boltzmann constant, T is the temperature of the gas, e is the charge of the ion, and E is the electric field strength (see e.g. [12]). Both the transverse and longitudinal diffusion coefficients are fitted with Equation (3) with the temperature T as a free parameter. The transverse diffusion corresponds to an effective temperature of 305 K, which is close to the gas temperature. The effective temperature of the longitudinal diffusion is rather high, 383 K. This could be explained by unrecognised minority carrier(s), or possibly spontaneous detaching of the electron from the CS_2^- ion, allowing the electron to drift for a short distance before being captured again by another CS_2 molecule. Alternatively, perhaps ions can change from a minority carrier(s) ion to a majority carrier(s) ion and back while drifting. A simple thermal model with a $1/\sqrt{E_{\text{drift}}}$ dependence describes the data well. In both cases, the main source of uncertainty is (local) temperature fluctuations and variations in the gas composition.

In other experiments using a low pressure CS_2 gas, the longitudinal diffusion is found to be in agreement with the thermal values [13]. In a 500 Torr He and 200 Torr CS_2 gas mixture, longitudinal diffusion coefficients slightly below to the thermal values are found [11].

4.4. Reconstruction of drift distance

The difference in drift velocity between the majority carrier and minority carrier(s) can be used to reconstruct the absolute position in the drift direction. Previously, this technique was demonstrated in a 30:10:1 Torr CF_4:CS_2:O_2 gas mixture with a spread on the reconstructed drift distance of ± 2 cm [4]. A precision of 16 mm was achieved using a similar technique using an SF_6 gas [14].

Here, fiducialisation is applied to data from the run at the largest drift field of 500 V/cm which gives the best signal peak separation, and also has the highest oxygen concentration of about 1150 ppm. About 4.4% of the hits are attributed to the minority carrier(s), whose mobility is 8.1% higher than that of the majority carrier.

The reconstruction proceeds by performing per event a binned maximum likelihood fit of Equation (1) to the measured relative arrival time of ions from one or more laser pulses. A new parameter t_0 is introduced to absorb the now unknown laser pulse time. The parameters f_2, r_2, f_{noise} are fixed to their previously fitted values. For σ_1 Equation (2) is used, and σ_2 is by approximation fixed to σ_1. The parameter μ_1 (the mean arrival time of the primary carrier peak) are acquired from the fit. The z-position is calculated using the measured drift velocity v_{drift}. The detected spread in the transverse direction is not utilised in the determination of the z-position.

By comparing the reconstructed z-position to the z-position of the laser stage for all six drift distances, the residual shown in Figure 9 is obtained. From a

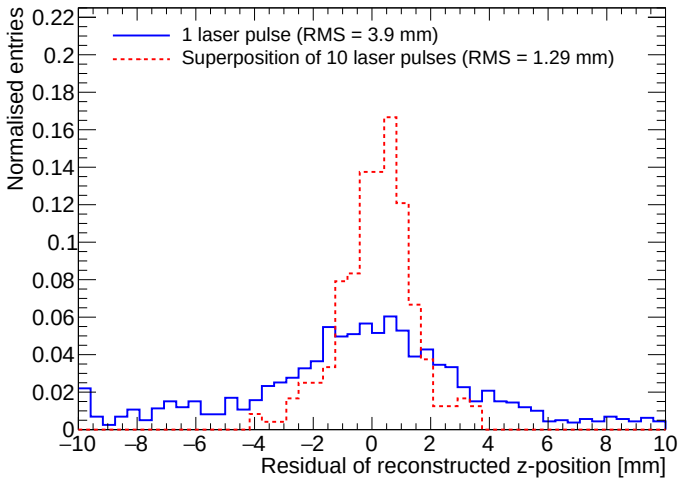

Figure 9: Residual of reconstructed z-position for 2401 laser pulses with a mean number of 43 detected ions and for 240 superpositions of ten laser pulses with a total mean number of 429 ions. The r.m.s. of the reconstructed z-positions for the single laser pulse is calculated for the 66% of the entries that fall inside the axis range.

single laser pulse, on average 43 ions are detected and the r.m.s. of the distribution is 3.9 mm for the 66 % of the laser pulses that fall within the ± 10 mm range. The determined z-position has a rather large spread, because very few minority carrier(s) ions are detected. In order to estimate the performance for a larger number of ions, a superposition of ten laser pulses at the same z-position is made by shifting their arrival times by the time difference between the laser pulses. From this we acquire emulated pulses with a mean total number of 429 detected ions of which about 19 ions are attributed to the minority carrier(s). This quantity of ions, the quad is still able to detect without occupancy problems. The resulting r.m.s. is 1.29 mm for the combined laser pulses and all of the entries are within the ± 4 mm range.

5. Conclusions and outlook

The performance of GridPix technology as a negative ion TPC readout was studied using a quad module with four Timepix3 based GridPix chips. The TPC is operated using a 93.6/5.0/1.4 gas mixture of $Ar/iC_4H_{10}/CS_2$ with a small amount of oxygen and water vapour at a pressure of 1030 mbar and a temperature of 297 K. Tracks were produced by a pulsed N_2 laser. The 1.56 ns time resolution of the Timepix3 chips allows for a precise determination of the drift properties in the longitudinal direction. The measured mobility is $(1.391 \pm 0.003)\,cm^2/V/s$. Using the high granularity pixel readout, the transverse and longitudinal diffusion coefficients were measured to correspond to an

effective thermal diffusion temperature of 305 K and 383 K respectively. A simple thermal model with a $1/\sqrt{E_{\text{drift}}}$ dependence describes the data well. This confirms the expected low diffusion coefficient for ions. Furthermore, the GridPix has an efficiency of approximately 60% to detect single drift ions. By using the relative arrival time of about 19 minority carrier(s) ions, the z-position can be measured with an expected precision of 1.29 mm.

In the future, a GridPix TPC readout might be of interest to directional dark matter experiments. The often desired operation at low pressure can be investigated in combination with a GridPix readout. For these experiments gas mixtures containing SF_6 have some advantages [13], and can also be studied for operation with a GridPix readout. Alternatively, for operation around atmospheric pressure replacing Argon with the lighter Helium could increase nuclear recoils lengths important for directional dark matter searches [15].

All in all, the fine granularity and high timing precision of the GridPix TPC readout in combination with a good single ion detection efficiency, provide an excellent position resolution in the longitudinal and transverse direction.

Acknowledgements

This research was funded by the Netherlands Organisation for Scientific Research NWO. The authors want to acknowledge the support of the mechanical and electronics departments at Nikhef.

References

[1] C. Martoff, D. Snowden-Ifft, T. Ohnuki, N. Spooner, M. Lehner, Suppressing drift chamber diffusion without magnetic field, Nucl. Instrum. Meth. A 440 (2000) 355–359. doi:10.1016/S0168-9002(99)00955-9.

[2] J. Battat, et al., Low Threshold Results and Limits from the DRIFT Directional Dark Matter Detector, Astropart. Phys. 91 (2017) 65–74. arXiv:1701.00171, doi:10.1016/j.astropartphys.2017.03.007.

[3] D. P. Snowden-Ifft, Discovery of Multiple, Ionization-Created Anions in Gas Mixtures Containing CS2 and O2 (8 2013). arXiv:1308.0354.

[4] J. Battat, et al., First background-free limit from a directional dark matter experiment: results from a fully fiducialised DRIFT detector, Phys. Dark Univ. 9-10 (2015) 1–7. arXiv:1410.7821, doi:10.1016/j.dark.2015.06.001.

[5] P. Colas, A. P. Colijn, A. Fornaini, Y. Giomataris, H. van der Graaf, E. H. M. Heijne, X. Llopart, J. Schmitz, J. Timmermans, J. L. Visschers, The readout of a GEM- or micromegas-equipped TPC by means of the Medipix2 CMOS sensor as direct anode, Nucl. Instrum. Meth. A535 (2004) 506–510. doi:10.1016/j.nima.2004.07.180.

[6] M. Campbell, M. Chefdeville, P. Colas, A. P. Colijn, A. Fornaini, Y. Giomataris, H. van der Graaf, E. H. M. Heijne, P. Kluit, X. Llopart-Cudie, J. Schmitz, J. Timmermans, J. L. Visschers, Detection of single electrons by means of a micromegas-covered MediPix2 pixel CMOS readout circuit, Nucl. Instrum. Meth. A540 (2005) 295–304. arXiv:physics/0409048, doi:10.1016/j.nima.2004.11.036.

[7] C. Ligtenberg, et al., Performance of the GridPix detector quad, Nucl. Instrum. Meth. A 956 (2020) 163331. arXiv:2001.01540, doi:10.1016/j.nima.2019.163331.

[8] T. Poikela, J. Plosila, T. Westerlund, M. Campbell, M. De Gaspari, X. Llopart, V. Gromov, R. Kluit, M. van Beuzekom, F. Zappon, V. Zivkovic, C. Brezina, K. Desch, Y. Fu, A. Kruth, Timepix3: a 65K channel hybrid pixel readout chip with simultaneous ToA/ToT and sparse readout, JINST 9 (05) (2014) C05013.
URL http://stacks.iop.org/1748-0221/9/i=05/a=C05013

[9] B. van der Heijden, J. Visser, M. van Beuzekom, H. Boterenbrood, S. Kulis, B. Munneke, F. Schreuder, SPIDR, a general-purpose readout system for pixel ASICs, JINST 12 (02) (2017) C02040. doi:10.1088/1748-0221/12/02/C02040.

[10] F. Hartjes, A diffraction limited nitrogen laser for detector calibration in high energy physics, Ph.D. thesis, University of Amsterdam (1990).
URL https://www.nikhef.nl/~i56/Thesis%20FredH.pdf

[11] C. Martoff, R. Ayad, M. Katz-Hyman, G. Bonvicini, A. Schreiner, Negative ion drift and diffusion in a TPC near 1 bar, Nucl. Instrum. Meth. A 555 (2005) 55–58. arXiv:physics/0406114, doi:10.1016/j.nima.2005.08.103.

[12] W. Blum, L. Rolandi, W. Riegler, Particle detection with drift chambers, Particle Acceleration and Detection, Springer, 2008. doi:10.1007/978-3-540-76684-1.
URL https://www.springer.com/gp/book/9783540766834

[13] N. Phan, R. Lafler, R. Lauer, E. Lee, D. Loomba, J. Matthews, E. Miller, The novel properties of SF_6 for directional dark matter experiments, JINST 12 (02) (2017) P02012. arXiv:1609.05249, doi:10.1088/1748-0221/12/02/P02012.

[14] T. Ikeda, T. Shimada, H. Ishiura, K. Nakamura, T. Nakamura, K. Miuchi, Development of a Negative Ion Micro TPC Detector with SF_6 Gas for the Directional Dark Matter Search (4 2020). arXiv:2004.09706.

[15] E. Baracchini, G. Cavoto, G. Mazzitelli, F. Murtas, F. Renga, S. Tomassini, Negative Ion Time Projection Chamber operation with SF_6 at nearly atmospheric pressure, JINST 13 (04) (2018) P04022. arXiv:1710.01994, doi:10.1088/1748-0221/13/04/P04022.